U-Pb Detrital Zircon, Geochemical and Nd isotope Constraints on Sedimentary Provenance of the Chewings Range Quartzite, Warumpi Province, Arunta Region, NT

Joshua Trestrail

Supervisors: Karin Barovich

Martin Hand

October 2010

Abstract

The Chewings Range Quartzite is a meta-sedimentary cover sequence located in the Warumpi Province of the Arunta Region. U-Pb detrital Zircon analysis of the Chewings Range Quartzite indicates a minimum depositional age of ~ 1640Ma, with the main population of zircons residing within a range of 1700 – 1800Ma. Evidence from Sm-Nd isotopic data suggests that a series of Staurolite Garnet Schists, often grouped with the Chewings Range Quartzite, has a significantly more juvenile character. This suggests that it may represent a new unit with a significantly differing provenance to that of the Chewings Range Quartzite. Combined REE, geochemistry and detrital zircon dating suggests that the Chewings Range Quartzite was derived primarily off the Arunta Region and North Australian Craton, while the Stauralite Garnet Schists holds more affinity with juvenile Musgrave Province to the south.

Table of Contents

1. Introduction

This report seeks to ascertain the provenance of the Chewings Range Quartzite, the upper metasedimentary unit of the Iwupataka Metamorphic Complex, Warumpi Province in the Arunta Region of Northern Australia (Scrimgeour et al. 2005b; Neumann et al. 2007). Sedimentary rocks are formed from the eroded detritus of other rocks. The study of provenance involves the analysis of a sedimentary rock to discover the source region(s) from which its sediments have been derived. To constrain the provenance of the Chewings Range quartzite three analytical tools have been used. These are U-Pb detrital zircon dating, geochemistry and Nd isotopes. The utilisation of several tools in Sedimentary provenance is important as each tool has its limitation. For example geochemical analysis can give you a "fingerprint" to identify a source terrain but it does not give you any information about the age of the sediment. The chemistry of a sedimentary rock is primarily controlled by the original composition of the source rocks or provenance (Taylor and McLennan 1985; McLennan et al. 1993; McLennan et al. 2003). This makes geochemistry a useful tool in provenance, allowing you to compare the elemental "fingerprint" of the sediments with that of prospective source terrains. This approach is based on the assumptions that the distributions of a number of trace elements are sensitive to the nature of the provenance and that these elements are retained in particular matter (Taylor and McLennan 1985; McLennan et al. 2003). In particular the distribution of Rare Earth elements (La-Lu) in sedimentary rocks is considered to faithfully reflect the character of the provenance (Taylor and McLennan 1985; McLennan et al. 2003). Other examples include high feild strength elements such as Zr, Nb, Y, Th and U which are preferentially partitioned into melts during crystallization (Feng and Kerrich 1990) and as a result these elements are enriched in felsic rather than mafic sources. Due to their relatively immobile behaviour in the sedimentary process they can also be used to reflect province composition (Taylor and McLennan 1985). However care must be taken as most elements can undergo some form of mobilization or fractionation under the right conditions during weathering, transport or diagenesis (McLennan et al. 2003). These factors can result in reduced accuracy or incorrect identification of provenance; however consideration of these effects in data analysis can still result in useful data. Sm–Nd isotopes, commonly used in conjunction with REE studies, provide an average provenance age and can be representative of the average composition of the provenance (McLennan et al. 1993; McLennan et al. 2003).

Zircon is an ultra-stable mineral that is resistant to changes in its internal chemistry, resulting in the preservation of zircons even through several recycling events (McLennan et al. 1993; McLennan et al. 2003). As the start of deposition must occur after the age of the youngest zircon (Howard et al. 2009), the use of detrital zircon U-Pb dating allows the placing of constraints on the age of maximum deposition for a given sedimentary unit (McLennan et al. 1993; Payne et al. 2006). In addition to this zircons may also record information on the timing of significant magmatic and metamorphic events in the source region (Payne et al. 2006). These factors allow zircons to be used to constrain a variety of crustal and tectonic processes including paleo-reconstruction models (McLennan et al. 1993; McLennan et al. 2003; Payne et al. 2006). The accuracy of U-Pb dating of zircons is dependent on the zircons remaining closed systems throughout their history. Unfortunately during thermal metamorphism zircon systems can be re-opened, which may lead to incorrect results. In order to determine if a population of zircons has been isotopically disturbed they can be plotted on a concordia graph. If the Zircons have been undisturbed they will plot on the concordia. However if the U-Pb ratios has been disturbed then they will plot on a straight line discordia (Howard et al. 2009). It is important to note that not all sources for sediments contain zircons. For example mafic rocks, carbonates and fine grained sedimentary rocks often contain little or no zircons, but may still be included in the provenance of the sediments (McLennan et al. 2003; Payne et al. 2006). Due to the strength of sedimentary provenance in constraining palaeogeographical reconstructions e.g (Ross et al. 1992; Stewart et al. 2001; Payne et al. 2006), for example by providing information about the proximity of various source regions at the time of deposition, another aim of this study is to provide constraints on the reconstruction of Proterozoic Australia.

Modern models for the reconstruction of Proterozoic Australia involve the assembly of various cratonic blocks colliding and accreting via subduction related processes (Myers et al. 1996; Karlstrom et al. 2001; Giles et al. 2002; Giles et al. 2004; Wade et al. 2006; Betts and Giles 2006). These models are supported by geochemical evidence indicating that subduction related process played a central role in the assembly of Proterozoic Australia (Zhao and Bennett 1995; Zhao and McCulloch 1995; Wade et al. 2006). This model was first outlined in detail by Myers et al. (1996), who proposed that three separate cratonic blocks (Fig.1) had independently formed prior to 1.83 Ga and were then accreted to each other by 1.3 Ga. Located on the southern margin of the North Australian Craton, the Arunta Region is ideally placed to help place constraints on the assembly of Proterzoic Australia. Several authors have suggested that arc like geochemical signatures in Arunta granites (Zhao and McCulloch 1995; Zhao and Bennett 1995) suggest a north dipping ~1.8 to 1.6 Ga subduction system eg (Karlstrom et al. 2001; Giles et al. 2002; Betts and Giles 2006). Recently the southern most province of the Arunta Region, the Warumpi province, has been interpreted as being exotic to the NAC, based on a lack of Archean inheritance in granites, younger

protolith ages and less evolved isotopic signatures (Scrimgeour 2004; Close et al. 2004; Scrimgeour et al. 2005b). The Warumpi Province was assumed to have been accreted onto the NAC at 1640 Ma during the Liebig Orogeny (Scrimgeour et al. 2005b). The series of major faults and shear zones which separate the Warumpi Province from the rest of the Arunta Region have been collectively termed the Central Australian suture by Close et al. (2004); Scrimgeour et al. (2005b); Scrimgeour et al. (2005a). This suture has been imaged to 150km depth by (Selway et al. 2009) using MT methods. The results of this imaging support the conclusion that the Warumpi province was accreted to the north Australian Craton due to a south dipping subduction event (Scrimgeour et al. 2005b; Wade et al. 2006; Selway et al. 2009). This model is in contrast to the previously mentioned models suggesting a North dipping subduction setting. The location of the Chewings Range Quartzite, within the Warumpi province, makes it ideally placed to help constrain future reconstruction attempts.

2. Geological Background

The Arunta Region (Fig.2) is a complex and extensively metamorphosed Proterozoic domain, located in the southern part of the North Australian Craton (Collins and Shaw 1995; Scrimgeour et al. 2005b). It contains an extensive tectonothermal history extending from the start of the Proterozoic to the end of the Palaeozoic (Collins and Shaw 1995). This area lies on the southern margin of the North Australian Craton. Recently (Scrimgeour 2004) has proposed a reclassification of the region into three distinct, fault bounded provinces based on differing protolith ages. The Warumpi Province is the southernmost province of the Arunta Region under this new classification scheme. Its extent is similar to the Southern Tectonic Province of Shaw et al. (1984).

The majority of the Warumpi Province is composed of two domains, the Yaya Domain in the north and the Haast Bluff Domain in the south and west. The oldest rocks in the Warumpi are felsic intrusive and extrusive rocks of the Haast Bluff Domain. The Haast Bluff Domain has been subdivided into the two sub-domains based on differences in metamorphic grade. In the east, the Glen Helen sub-domain has experienced upper amphibolite facies metamorphism, with the production of felsic migmatite within the Glen Helen Metamorphics, of the Madderns Yard Metamorphic Complex (Scrimgeour et al. 2005a). The timing of the migmitisation has been loosely attributed to the Liebig Orogeny (Kinny 2002; Scrimgeour et al. 2005a). The Kuta Kuta subdomain in the west has experienced lower amphibolite facies metamorphism, presumably during the 1590-1570Ma Chewings Orogeny (Scrimgeour et al. 2005a).

The Yaya Domain is comprised of a metsedimentary succession, contains pelites to psammites, calc-silicates and felsic to mafic granulite faces metamorphic rocks (Scrimgeour et al. 2005a; Scrimgeour et al. 2005b). It is thought to have been largely deposited between 1660Ma and 1640Ma. This metasedimentary sequence is a component of the Yaya Metamorphic Complex in addition to migmatic felsic and mafic gneisses. Granulite facies metamorphism of this complex is thought to have occurred during the Liebig Orogeny at 1640-1630Ma. (Scrimgeour et al. 2005a; Scrimgeour et al. 2005b).

The eastern part of the Warumpi Province was originally divided by Warren and Shaw (1995) into the basement Madderns Yard Metamorphic Complex and overlying Iwupataka Metamorphic Complex. The Madderns Yard Metamorphic Complex consists of upper amphibolite facies felsic gneisses, with minor metasedimentary rocks (Warren and Shaw 1995b; Scrimgeour et al. 2005b).

The Madderns Yard Metamorphic Complex is unconformable overlain by the 1640-1610 Ma Iwupataka Metamorphic Complex (Warren and Shaw 1995b; Zhao and Bennett 1995). This experienced lower amphibolites facies metamorphism. It is comprised of metasedimentary and possible metavolcanic rocks, with an upper quartzite unit, the Chewings Range Quartzite (Scrimgeour et al. 2005a). The intrusion of granites into the metasedimentary rocks of the Iwupataka Metamorphic Complex, with ages of 1603 +/- 7 Ma and 1603 +/- 11 Ma (Collins et al. 1995; Zhao and Bennett 1995), in addition to the presence of a possible metavolcanic body within the Iwupataka Metamorphic Complex with a SHRIMP U-Pb age of 1615 +/- 11 Ma(Zhao and Bennett 1995), provides a lower constraint on the deposition of this complex. Zircon dating of the Chewings Range Quartzite suggests a maximum depositional age constraint of 1669 ± 13 Ma (Scrimgeour et al. 2005a). However based on detrital zircon data from quartzite rocks in MOUNT RENNIE (Nguman Metamorphics), mapped as equivalents of the Iwupataka Metamorphic complex (Scrimgeour et al. 2005a), Scrimgeour et al. (2005a) has conditionally proposed a maximum depositional age of 1630Ma. Due to the uncertainty associated with the deposition of the Iwupataka Metamorphic Complex, Scrimgeour et al (2005a) has proposed two possible timings for its deposition.

1. The Iwupataka Metamorphic Complex was deposited before the Liebig Orogeny but was metamorphosed to a lower grade than potentially equivalent rocks in the Yaya Domain. This accounts for the lack of any significant zircon population associated with large scale 1640-1635Ma magmatism across the region.

2. The Iwupataka Metamorphic Complex was deposited after the Liebig Orogeny. This is consistent with the higher metamorphic grade of the Glen

Helen Metamorphics, which suggests the Glen Helen Metamorphics have experienced an additional metamorphic event.

It is considered that the Iwupataka Metamorphic Complex is more likely to have been deposited 1630-1610Ma (Scrimgeour et al. 2005a), though the possibility of deposition before the Liebig Orogeny cannot be excluded.

3. Sampling and Methods

The lithology of the Chewings Range Quartzite is dominated by a massive metamorphosed quartzite sandstone (Warren and Shaw 1995a). Extensive interlaid schist bands, within sections of the quartzite, result in a wide range of lithological expressions, ranging from silica rich outcrops of muscovite/staurolite-garnet bearing schists to extensively layered and crenulated mica rich quartzite (Teyssier et al. 1988; Warren and Shaw 1995a). Due to the tendency of REE to be concentrated in fine grained sediments and suggestions that they are more likely to represent a homogeneous source mixture (Condie et al. 1992; Cullers and Podkovyrov 2000; Tran et al. 2003), such sediments are often preferred targets for analysing geochemical provenance using REE. The distribution of REE and trace elements in coarse – grained sediments may be influenced by sedimentary sorting processes (Feng and Kerrich 1990; McLennan et al. 2003) and as a result the geochemistry of coarse grained sediments may not truly reflect source composition, however coarser grain sediments are also more likely to contain enough zircons to provide a representative population, sufficient in size to be analytically valid (Anderson 2005; Barovich and Hand 2008). For these reasons samples were taken from as wide a range of potential lithologys as possible, in order to provide the highest possibility of positive results.

Samples of whole rock were cut to remove weathered surfaces, then crushed and powdered in a tungsten carbide mill. These powders were sent to Amdel Laboratories for major and trace element geochemical analyses. A small amount of the rock powder was retained for Sm-Nd isotope analyses at the University of Adelaide isotope laboratory. Details of the Sm-Nd isotope method are as given in (Payne et al. 2010). Sub 0.1g powdered whole rock samples were spiked with a 150Nd/147Sm solution before the addition of HF/HNO3. The samples were evaporated overnight in Teflon "bombs" before being oven-heated at 190C for 5 days in HF within sealed Teflon and steel bombs. The HF was then evaporated during the day, with HNO3 added before the samples completely dried. HCL was added to the samples, which were bombed at 160C for a further 2 days before the HCL was evaporated. Two-stage exchange

columns were used to separate the Sm and Nd, which were subsequently analysed with the use of a Finnegan MAT 262 TIMS. Single grain U-Pb Zircon dating was undertaken following the method given in (Payne et al 2006) with the exception that the in-house standard Plesovice (Sláma et al. 2008) was utilized instead of the Sri Lankan zircon standard (BJWP-1).

4. Geochemistry and Sm-Nd isotopes

4.1 Major and trace element geochemistry

Whole rock geochemistry data is displayed in Tables 1 and 2. The Chewings Range Quartzite shows significant lithological variation across the pelite-psammite spectrum, this is well represented by the inverse linear relationship between SiO_2 and Al_2O_3. The distinct lack of samples in the 71% - 82% SiO_2 range is taken to represent the transition from pelitic to psammitic samples. The pelites fall within a SiO_2 range of 57.3 – 70.3 wt %, with average Ni, Cr and Sc concentrations of 21.25, 105.9 and 15.625 ppm respectively. These values are comparable to those of PAAS(Cr = 110 ppm and Sc = 16ppm) with the exception that Ni is uniformly lower than PAAS (Ni = 55ppm). It must also be noted that values for Cr have a significant range (45 – 160ppm). In comparison the psammite samples respectively show average Ni, Cr and Sc concentrations of 2.8, 82.7 and <5 ppm. High field strength elements Zr, Y and Nb average 157, 25.1875 and 11.6875 ppm respectively in the pelites. One sample (CHW09-14) has an abnormally high Zr concentration (410ppm), while the rest of the pelites lie within a range of 105 – 220ppm, this sample was not included in the average. Average concentrations of high field strength elements Y and Nb in the psammites are significantly lower (5.1 and 2.6 ppm respectively) than those observed in the pelites. On the other hand the psammites are slightly more enriched in Zr (165.7 ppm) if two outliers (STC09 -12 Zr= 30 ppm and STC09-21 Zr = 35ppm) are removed. Total abundance of REE's average 218.2ppm (Range 138 -281 ppm) for the pelites, while ∑REE for the Psammites is much lower at 99.9 ppm (Range 33 – 160 ppm). The reduced abundance of Rare Earth elements in the psammites, over the pelites, is due to quartz containing little or no REE (Taylor and McLennan 1985). Both the pelites and psammites also follow a trend of decreasing trace element concentration with increasing SiO_2 content (Fig.3), which can be attributed to the quartz dilution effect (Slack and Steven 1994). Variations in REE and other trace element concentrations may also be due to heavy mineral sorting, where the distribution of minerals such as monazite, apatite and zircon are preferentially sorted during sedimentary processes. (McLennan et al. 1993; Bea 1996). One way to quantify part of this effect is a plot of Th/Sc vs. Zr/Sc ratios (Fig.4). In igneous

processes Th and Sc are incompatible and compatible respectively; in addition they are not redistributed during sedimentary processes and hence act as indicators of provenance (McLennan et al. 1993). The compositional line was defined by (McLennan et al., 1993) using data from active margin samples, with little evidence of sedimentary sorting and recycling. Scatter around this line can be attributed to differences in provenance; however zircon concentration as a result of sedimentary recycling and sorting would enrich Zr relative to Th. The majority of the samples plot along the compositional line. However several samples have an enhanced Zr/Sc ratio with respect to Th/Sc. The effects this has on REE distributions within these samples will be discussed further in this report. Chondrite normalised REE patterns are presented in Figure 5. The pelites and psammites both show generally similar REE patterns, with LEE enrichment, negative Eu anomaly and a predominantly flat HREE enrichment. The psammites show significantly less enrichment than the pelitic samples, especially in regards to HREE and are also display a significantly more fractionated pattern with an average (La/Yb)n of 25 compared to the average of 7.8 for pelite samples. There are two exceptions to this trend, both samples STC09 - 12 and STC09 - 21 are depleted in HREE with regard to chondritic meteorites. Due to the high silica content of these samples, 97.8% SiO_2 and 99.1% SiO_2 respectively, the likely cause of these anomalies is extreme quartz dilution as discussed previously. These two samples also show a spike in Tm in regards to other HEE, this is due to both samples having Tm concentrations below detection limit. Pelite samples express a trend that mirrors that of PAAS, with the exception of slight variations in HREE enrichments.

4.2 Sm-Nd isotopic data

Results of Sm-Nd isotopic analysis of 9 samples of the Chewings Range Quartzite is presented in Table. 3 and Figure. 5 and 6. The estimated maximum depositional age (1640Ma), as determined by geochronology, is used to calculate the initial εNd values. The results can be broadly split into two main groups. The first, composed of predominantly psammites, have a εNd(T) range of -3.91 to -3.67 corresponding to an average Nd^{TDM} of 2342 Ma. The second group contains only pelites and has a εNd(T) range of 2.52 to 3.66 corresponding to an average of 1876 Ma. A single remaining analysis has a εNd (T) value of 0.31 and Nd^{TDM} of 2056 Ma.

4.3 U-Pb detrital Zircon Geochronology

Detrital U-Pb age data was obtained from two samples of the Chewings Range Quartzite. The resulting spectra, composed of analyses with less than 10% discordance, are presented in Figure 7. Most of zircons analysed fall within the range 1650 – 1850 Ma with a mode of 1750 - 1770Ma. Both samples contain a secondary peak at ~2520 – 2530 Ma and one sample displays another minor peak at 2050Ma. The majority of zircons were mostly detrital, showing oscillatory zoning and lack of any observable metamorphic overgrowths (Fig. 8 and 9).

5. Discussion

5.1 Analysis of Geochemical patterns

The deviation of several psammite samples from the expected compositional trend on a Th/Sc versus Zr diagram (Fig.3) indicates that these samples have been potentially enriched in heavy minerals, such as zircon and monazite, as a result of sedimentary recycling and sorting. These heavy elements can potentially represent a significant portion of the REE budget in a given sedimentary rock (Taylor and McLennan 1985), as such enrichment of these minerals may impact the integrity of REE patterns and the results of Sm-Nd isotopic analysis. Several methods can be used to quantify the impact of heavy mineral enrichment on the geochemistry of the samples and thus ensure that REE patterns and Sm-Nd isotopic values represent those of the source. Assuming the majority of Zr is contained within zircon then 100ppm of Zr will contribute less than 0.5 x Chondritic levels of heavy REE (Taylor and McLennan 1985). The three samples CHW09 – 01, CHW09 – 8 and CHW09 – 12 show the most Zircon enrichment relative to Th/Sc. These samples have Zr concentrations of 210, 245 and 110 ppm respectively. The average HREE content of these three samples is approximately 4 times chondritic values. Given these values, in the worst case scenario zircons will account for ~ 20% of the total HREE budget in samples showing heavy REE enrichment. If the assumption that Zr is concentrated in zircon, and hence affecting the HREE distributions in the rock, is correct then a plot of Zr against the (La/Yb)n ratio should show a correlation between the two values (Barovich and Hand 2008). However both the pelites and psammites show moderate scatter (Fig.10). Due to the significantly greater affinity of zircons for HREE over LREE, even if zircons provide a significant control on the HREE distribution, the distribution of LREE should remain unaffected, especially considering that the concentration of LREE elements in the psammite samples is significantly higher than the corresponding concentrations of HREE. Distributions of LREE may be influenced by the heavy mineral monazite, which is strongly enriched in LREE (Gromet and Silver 1983). The lack of a significant correlation between Th and (La/Yb)n ratio suggests that any potential monazite enrichment does not contribute greatly to the LREE budget in

affected samples (Barovich and Hand 2008). Furthermore the relationship between Al2O3 and Zr, Th and (Gd/Yb)n show moderate correlations for both pelite and psammite samples. This is consistent with trace element abundances being controlled in part by the initial clay minerals in the samples (Taylor and McLennan 1985). Due to these factors it is considered unlikely that the HREE patterns of the psammite samples have been adversely affected to a significant degree due to heavy mineral sorting, however the possibility cannot be completely ruled out.

5.2 Geochemistry and Sm-Nd isotopes: a case for a new unit?

As a whole the pelites share a similar geochemistry and REE trend (Fig. 10), and with a few exceptions tend to be more LREE enriched than PAAS. However despite this geochemical similarity the results of the Sm-Nd isotopic analysis show two strikingly different distributions. The first distribution has a εNd (1640 Ma) range of -3.91 to -3.67 and encompasses both psammite and pelite samples. The second distribution has a more juvenile isotopic signature with a εNd(1640 Ma) range of +3.66 to +2.52. These juvenile isotopic signatures are from samples of Staurolite Granet Schists associated with the Chewings Range Quartzite. Previously these outcrops have been included within descriptions of the Chewings Range Quartzite (Warren and Shaw 1995a). A small range of εNd (T) values (eg. 0-3), and sometimes even larger ranges, are not unusual within a sedimentary package (Maas and McCulloch 1991; Hurowitz and McLennan 2005; Payne et al. 2006). However the rather extensive difference in End range and the spatial grouping between groups of significantly differing End value is indicative of a significant difference in provenance between these samples. For this reason the provenance of the Staurolite Garnet Schists will be considered separately from that of the Chewings Range Quartzite. The extent of the Stauralite Garnet Schist will be considered roughly analogous to the combined muscovite schist and the Stauralite Garnet Schist mapped as part of the Chewings Range Quartzite in (100k ALICESPRINGS Map).

5.3 Provenance of the Chewings Range Quartzite

As mentioned previously the HREE signature of the psammite samples within the Chewings Range quartzite may have been disturbed by heavy mineral enrichment. With this in mind the REE patterns of the pammite samples are roughly comparable to those displayed by Southern Arunta Granites, in particular the HHP and main groups as described by (Zhao and Bennett 1995). In general the psammite samples tend to have a slightly higher La/Yb ratio than the majority of the main and HHP group granites. This difference in La/Yb ratio however can be explained by the presence of the CAT group of granites, also located in the Southern Arunta, which are characterised by high La/Yb ratios. As such the REE patterns of the psammite samples compare favorably to those of the southern Arunta Granites, assuming an

averaging of the source components. The distinctive flat HREE trends and enrichment in LREE characteristic of much of the main and HHP groups are also comparable to similar trends displayed by the pelite samples. Similar trends seen in Amadeus Basin sediments have been suggested by Zhao (1992) to be characteristic of Arunta Block granites. Both pelites and psammites display a moderate to large Eu Anomaly(fig.), suggestive of a source region that may have been affected by intracrustal melting processes (Taylor and McLennan 1985; Barovich and Hand 2008). This is consistent with an Arunta source for these sediments. Geochemical provenance indicators (Fig. 11) show the similarity between the psammite samples and Arunta granites, while pelites tend to be closer in character to Mt Isa, a terrain of similar age to the Arunta, also located on the North Australia craton (McDonald et al. 1997; Page and Sun 1998). This difference in geochemistry may suggest that the pelites are more representative of a homogeneous NAC source. The geochronology results obtained during this study compare favourably with the results obtained by (Scrimgeour et al. 2005a) (fig.7). The youngest zircon analysed in this study is 1641 Ma +/- 21. This is similar to the average of the six youngest zircons reported by (Scrimgeour et al. 2005a) - 1669 ± 13 Ma. The majority of the zircon ages fall over a palaeoproterozoic age range of 1700 – 1800 Ma, with a mode of 1740 – 1770 Ma. This age range is very characteristic of the granite suits in the Arunta Province, the majority of which were intruded at 1750 – 1770 Ma (Zhao and Bennett 1995). The small imput of ~1900Ma age zircons may be sourced from Mt Isa, if as the provenance indicators suggest, it forms part of the source for the Chewings Range Quartzite. The small 2100 – 2200 Ma and ~2500 Ma zircon signals in the Chewings Range Quartzite is also present in the widespread clastic sediments of the Arunta block (Claoue-Long et al. 2005). The εnd evolution of the Arunta block, Mt Isa and the Gawler Craton along with the End values obtained during this study can be found in (Fig. 12). The εNd(1640 Ma) range of -3.91 to -3.67 for the Chewings Range Quartzite plots within the isotopic evolution of the Arunta Region. Based on the combined geochemical and geochronological data the Arunta Region, and in particular the Southern Arunta granites seem to be the preferred source region for the Chewings Range Quartzite. Potentially with minor input from Mt Isa and the rest of the NAC.

5.4 Provenance of the Staurolite – Garnet – Schist

With a εNd(T) range of + 3.66 to + 2.52 T=1640Ma, The Stauralite – Granet Schist has a significantly more juvenile isotopic signature than the rest of the Chewings Range Quartzite (Table. 3). These values also lie outside the range for averaged Arunta lithologies e.g. (-9.5 to -1.1) for εNd(1.6 Ga) (Payne 2006). However there are juvenile mafic amphibolites associated with the southern Arunta granites, not included in the previous averaging due to their comparatively minor volume, with comparable εNd values to those of the staurolite garnet schists (Zhao 1994). The

group 1 amphibolites as described by Zhao (1994) have a εnd(T) range of +4.2 to +5.1 at (T=1770 Ma). Despite this isotopic similarity the REE trends for Group 1 amphibolites show flat to LREE depleted patterns, which is dissimilar to the REE trends displayed by the Staurolite Garnet Schists. In addition the minor comparative volume of these juvenile lithologies limits their potential contribution to the provenance of the Staurolite Garnet Schists. These factors would seem to rule out the Arunta region as a potential source, despite the geochemical similarities between Stauralite Garnet Schists and the Chewings Range Quartzite. This necessitates a search for a more juvenile terrain that could form the source for these sediments. One potential source is the Musgrave Province, which is a 1.60 – 1.08 Ga Proterozoic terrain located in central Australia, south of the Arunta Province and Amadeus basin (Wade et al. 2006). If the Staurolie Garnet Schist dose represents a new distinct unit from the Chewings Range Quartzite, then the age constraints on the Chewings Range Quartzite might not be applicable to the Staurolite Garnet Schists. In which case the minimum deposition age of the Staurolite Garnet Schist is constrained by recent dating of garnets and monazites to give a deformation age of ~ 1140 Ma (unpublished data). A recalculation of εnd(T) with T = 1140Ma gives a range of - 2.59 to – 1.65 , which is anglous to values for the Musgrave Province (Fig.12). In particular the Pitjantjatjara Supersuite, which comprises a significant area of the northern Musgraves, may be a viable source for sediments deposited at (~1140 Ma). Unfortunately there is limited available geochemistry on the rocks comprising the Pitjantjatjara Supersuit (Wade et al. 2008). As such there is currently no overreaching detailed geochemical study available, which limits the effectiveness of comparing the geochemical characteristics of the Pitjantjatjara super suit and the Staurolite Garnet Schist. If the provenance of the Staurolite Garnet Schist is linked to the Pitjantjatjara Supersuite then this would imply the Chewings Range Quartzite was exhumed or at least locally exposed at some point during the 1.23 – 1.15 Ga Musgrave Orogeny (Wade et al. 2008). The close age association between the deformation of the Staurolite Garnet Schist at 1140Ma and the Musgrave Orogeny however suggests that it may have been deformed during the Musgrave Orogeny, which would indicate a depositional age older than that of the Pitjantjatjara Supersuite (1.22 – 1.14 Ma). Identification of a source terrain for the Staurolite Garnet Schist is hampered by the lack of geochronoical data and depositional constraints. However based on its Juvenile isotopic signature the Musgrave province is considered to be the most promising candidate.

Conclusions

The following conclusions can be drawn from this study:

1. Based on geochronological, geochemical and Nd isotopic signatures it is believed that the most likely source for the Chewings Range Quartzite is the Arunta Province, in particular the southern Arunta Granite suites.

2. A highly Juvenile Staurolite Garnet Schists, previously associated with the Chewings Range Quartzite have a highly juvenile isotopic signature similar to that of the Warumpi Province.

Acknowledgments

I would like to thank my supervisor Karin Barovich for her support and help as well as great thanks to Martin Hand for collecting many of my samples in the summer time heat. The technical traning provided by Ben Wade and David Bruce in the use of the LA-ICPMS and the TIMS was also greatly apreciated. Justin Payne also deserves a mention for his aid in anaysing my giliter data among other deeds. Finaly a big thanks to my family and friends for their support and encouragment throughout this year.

Appendix

See Below References

References

ANDERSON T. 2005 Detrital zircons as tracers of sedimentary provenance: limiting conditions from statistical and numerical simulations, *Chemical Geology,* vol. 216, pp. 29-270.

BAROVICH K. M. & HAND M. 2008 Tectonic setting and provenance of the Paleoproterozoic Willyama Supergroup, Curnamona Province, Australia: Geochemical and Nd isotopic constraints on contrasting source terrain components, *precambrian Research*

BEA F. 1996 Residence of REE, Y, Th and U in granites and crustal protoliths; implications for chemistry of crustal melts, *Journal of Petrology,* vol. 37, pp. 521-552.

BETTS P. G. & GILES D. 2006 The 1800 - 1100 Ma tectonic evolution of Australia, *Precambrian Research,* vol. 144, pp. 92-125.

CLAOUE-LONG J.*, et al.* 2005 Towards a Correlation of the earliest Proterozoic evolution in Central Australia, *Northern Territory geological Survey 2005 Abstracts*.

CLOSE D. F.*, et al.* 2004 Late Palaeo-proterozoic development of the SW margin of the North Australian Craton, *Geological Society of Australia,* vol. 73 (Abstracts), p. 149.

COLLINS W. J. & SHAW R. D. 1995 Geochronological constraints on orogenic events in the Arunta Inlier: a review, *Precambrian Research,* vol. 71, pp. 315-346.

COLLINS W. J.*, et al.* 1995 The age of the Ormiston Pound Granite: implications for Mesoproterozoic evolution of the Arunta Inlier, central Australia, *Precambrian Research,* vol. 71, pp. 91-105.

CONDIE K. C., NOLL P. D. & CONWAY C. M. 1992 Geochemical and detrital mode evidence for two sources of Early Proterozoic metasedimentary rocks from the Tonto Basin Supergroup, central Arizona, *Sedimentary Geology,* vol. 77, pp. 51-76.

CULLERS R. L. & PODKOVYROV V. N. 2000 Geochemistry of the Mesoproterozoic Lakhanda shales in southeastern Yakutia, Russia: implications for mineralogical and provenance control, and recycling, *Precambrian Research,* vol. 104, no. 77-93.

FENG R. & KERRICH R. 1990 Geochemistry of shales from the Archean Abitibi greenstone belt, Canada: Implications for provenance and tectonic setting, *Geochimica et Cosmochimica Acta,* vol. 54, pp. 1061-1081.

GILES D., BETTS P. G. & LISTER G. 2002 Far-feild continental backarc setting for the 1.80-1.67 Ga basins of northeastern Australia, *Geology,* vol. 30, pp. 823-826.

GILES D., BETTS P. G. & LISTER G. 2004 1.8-1.5 Ga links between the north and south Australian cratons and the early-middle Proterozoic configuration of Australia, *Tectonophysics,* vol. 380, pp. 27-41.

GROMET L. P. & SILVER L. T. 1983 Rare earth element distributions amoung minerals in a granodiorite and their petrogenetic implications., *Geochimica et Cosmochimica Acta,* vol. 47, pp. 925-939.

HOWARD K. E.*, et al.* 2009 Detrital zircon ages: Improving interpretation via Nd and Hf isotopic data, *Chemical Geology*.

HUROWITZ J. A. & MCLENNAN S. M. 2005 Geochemistry of Cambro-Ordovician sedimentary rocks of the Northeastern United States: changes in sediment sources at the onset of Taconian orogenesis, *Journal of Geology*, no. 113, pp. 571-587.

KARLSTROM K. E.*, et al.* 2001 Long-lived (1.8-1.0 Ga) convergent orogen in southern Laurentia, its extensions to Australia and Baltica, and implications for refininf Rodinia, *Precambrian Research,* vol. 111, pp. 5-30.

KINNY P. D. 2002 SHRIMP U-Pb geochronology of Arunta Province samples from the Mount Liebig and Lake Mackay 1:250 000 mapsheets., *Northern Territory geological Survey, Technical Note*.

MAAS R. & MCCULLOCH M. T. 1991 The Provenance of Archean clastic metasediments in the Narryer Gneiss Complex, Western Australia trace-element geochemistry, Nd isotopes and U-Pb ages for Detrital Zircons, *Geochimica et Cosmochimica Acta,* vol. 55, pp. 1915-1932.

MCDONALD G. D., COLLERSON K. D. & KINNY P. D. 1997 Late Archean and Early Proterozoic crustal evolution of the Mount Isa block, northwest Queensland, Australia, *Geology,* vol. 25, pp. 1095–1098.

MCLENNAN S. M.*, et al.* 2003 The roles of provenance and sedimentary processes in the geochemistry of sedimentary rocks.

--- 1993 Geochemical approaches to sedimentation, provenance and tectonics, *Geological society of America Special Paper 284*.

MYERS J. S., SHAW R. D. & TYLER I. M. 1996 Tectonic evolution of Proterozoic Australia, *Tectonics,* vol. 15, pp. 1431-1446.

NEUMANN N., FRASER G. L. & GEOSCIENCE A. 2007 Geochronological synthesis and time-space plots for Proterozoic Australia / Narelle L. Neumann and Geoffrey L. Fraser editors. Geoscience Australia, Canberra.

PAGE R. W. & SUN S. S. 1998 Aspects of geochronology and crustal evolution in the Eastern Fold Belt, Mt Isa Inlier, *Australian Journal of Earth Sciences,* vol. 45, pp. 343-361.

PAYNE J. L., BAROVICH K. M. & HAND M. 2006 Provenance of metasedimentary rocks in the northern Gawler Craton, Australia: Implications for Palaeoproterozoic reconstructions, *Precambrian Research*.

PAYNE J. L., *et al.* 2010 Pitfalls of Classifying ancient magmatic suites with tectonic discrimination diagrams: An example from the Paleoproterozic Tunkillia Suite, southern Australia, *Precambrian Research,* vol. 177, pp. 227-240.

--- 2008 Temporal constraints on the timing of high-grade metamorphism in the northern Gawler Craton: implications for assembly of the Australian Proterozoic., *Australian Journal of Earth Sciences,* vol. 55, pp. 623-640.

ROSS G. M., PARRISH R. R. & WINSTON D. 1992 Provenance and U-Pb geochronology of the Mesoproterozoic Belt Supergroup (Northwestern United States) - implications for age of deposition and Pre-Panthalassa plate reconstructions., *Earth Planet*.

SCRIMGEOUR I. R. 2004 A revised province definition and Palaeoproterozoic framework for the Arunta Region, central Australia, *Geological Society of Australia (Abstracts)*.

SCRIMGEOUR I. R., CLOSE D. F. & EDGOOSE C. J. 2005a Mount Liebig, Northern Territory. 1:250 000 geological map series explanatory notes, SF 52-16.: Northern Territory Geological Survey, Darwin and Alice Springs.

SCRIMGEOUR I. R., *et al.* 2005b High-T granulites and polymetamorphism in the southern Arunta Region, central Australia: Evidence for a 1.64 Ga accretional event, *Precambrian Research,* vol. 142, no. 1-2, pp. 1-27.

SELWAY K., *et al.* 2009 Magnetotelluric constraints on subduction polarity: Reversing reconstruction models for Proterozoic Australia, *Geology,* vol. 37, no. 9, pp. 799-802.

SHAW R. D., STEWART A. J. & BLACK L. P. 1984 The Arunta inlier: a complex ensialic mobile belt in central Australia, Part 2 Tectonic history, *Australian Journal of Earth Sciences,* vol. 31, pp. 457-484.

SLACK J. F. & STEVEN B. P. 1994 Clastic metasediments of the Early Proterozoic Broken hill Group. New south Wales, Australia: geochemistry provenance, and metallogenic significance., *Geochimica et Cosmochimica Acta,* vol. 58, pp. 3633-3652.

SLÁMA J., *et al.* 2008 Plešovice zircon - A new natural reference material for U-Pb and Hf isotopic microanalysis, *Chemical Geology,* vol. 249, no. 1-2, pp. 1-35.

STEWART J. H., *et al.* 2001 Detrital Zircon provenance of Mesoproterozoic to Cambrian arenites in the western United States and northwest Mexico, *Geological society of America*.

TAYLOR S. R. & MCLENNAN S. M. 1985 The Continental Crust: Its Composition and Evolution, *Blackwell Scientific, Oxford*.

TEYSSIER C., AMRI C. & HOBBS B. E. 1988 South Arunta Block: The internal zones of a Proterozoic overthrust in Central Australia, *Precambrian Research,* vol. 40/41, pp. 157-173.

TRAN J. T., *et al.* 2003 Nd isotope and geochemical constraints on the depositional setting of Paleoproterozoic metasedimentary rocks along the margin of the Archean Hearne craton, Saskatchewan, Canada, *Precambrian Research,* vol. 123, pp. 1-28.

WADE B. P., *et al.* 2006 Evidence for early Mesoproterozoic arc magmatism in the Musgrave Block, central Australia: Implications for Proterozoic crustal growth and tectonic reconstructions of Australia, *Journal of Geology,* vol. 114, pp. 43-63.

--- 2008 The Musgrave Province: Stitching north, west and south Australia, *Precambrian Research,* vol. 166, pp. 370-386.

WARREN R. G. & SHAW R. D. 1995a 1:250000 Geological Map Series Explanatory Notes HERMANNSBURG, *Northern Territory geological Survey*.

--- 1995b Hermannsburg, Northern Territory SF53-13. 1:250 000 geological map series explanatory notes. . Northern Territory Geological Survey, Darwin.

ZHAO J. 1994 Geochemical and Sm-Nd isotopic stuy of amphibolites in the southern Arunta Inlier, central Australia: evidence for subduction at a Proterozoic continental margin, *Precambrian Research,* vol. 65, pp. 71-94.

ZHAO J. & BENNETT V. C. 1995 SHRIMP U-Pb zircon geochronology of granites in the Arunta Inlier, central Australia: implications for Proterozoic crustal evolution, *Precambrian Research,* vol. 71, pp. 17-43.

ZHAO J. X. & MCCULLOCH M. T. 1995 Geochemical and Nd isotopic systematics of granites from the Arunta Inlier, central Australia: Implications for Proterozoic crustal evolution, *Precambrian Research,* vol. 71, pp. 265-299.

Appendix

Figure 1: Model showing proposed north dipping subduction beneath North Australia craton (NAC and model for its Amalgamation with south Australian Craton SAC to form the Musgrave Block, From Selway et al. (2009).

Figure 2: Map of Arunta region, insert shows location of Arunta on the NAC, From Scrimgeour et al. (2005b).

Figure 3: Both the Psammite and Pelites show a trend of decreasing trace element concentration with increasing SiO2 content.

Figure 4: Th/Sc versus Zr/Sc as per McLennan et al. (1993). The compositional variation line (approximate) shows the general trend expected due to variations in source composition.

Figure 5: REE diagram with both psammites and pelites

Figure 6: REE diagram contrasting Pelite samples with PAAS

Figure 7: Geochronical spectrum for analysed samples of the Chewings Range Quartzite (top). Bottom spectrum from Scrimgeour et al. (2005a).

Figure 8: Examples of zircons from CHW 09 -8.

Figure 9: Examples of Zircons from CHW 09 – 12.

Figure 10: Plot of Zr against the (La/Yb)n ratio, moderate scatter within individual groups indicates that Zr may not be a strong control on HREE distribution.

Figure 11: Geochemical provenance indicators as per Barovich and Hand (2008).

Figure 12: End versus time with the Chewings range ploted at estimated time of deposition, diagram as per Barovich and Hand (2008).

Figure 13: End versus time for the Staurolite Garnet Schists, (pelites). Values ploted for both T = 1640Ma and T = 1140Ma.

Table 1: Bulk Geochemistry of pelites.

Table 2: Bulk Geochemistry of Psammites.

Table 3: End Summary.

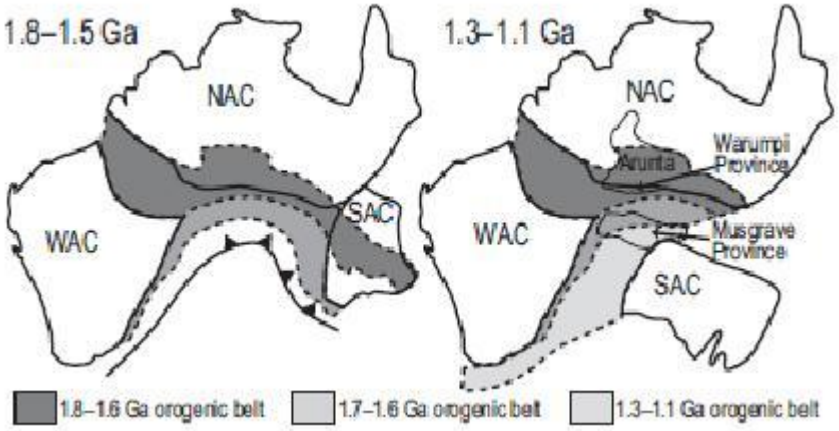

Figure. 1

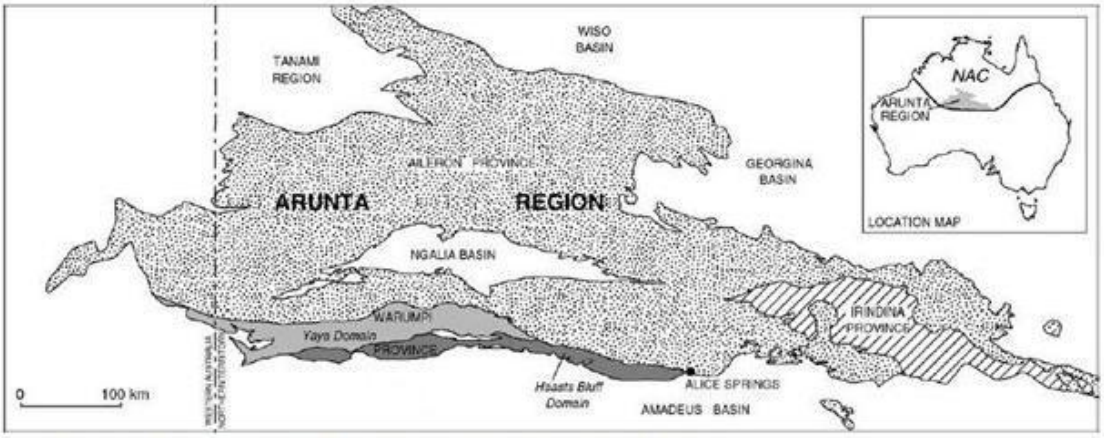

Figure. 2

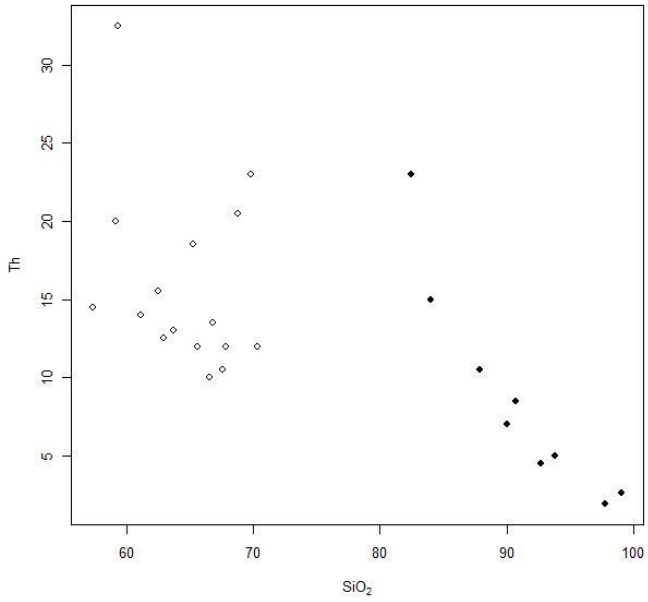
Th
30
25
20
15
10
5
60
70
80
90
100
SiO2

Figure. 3

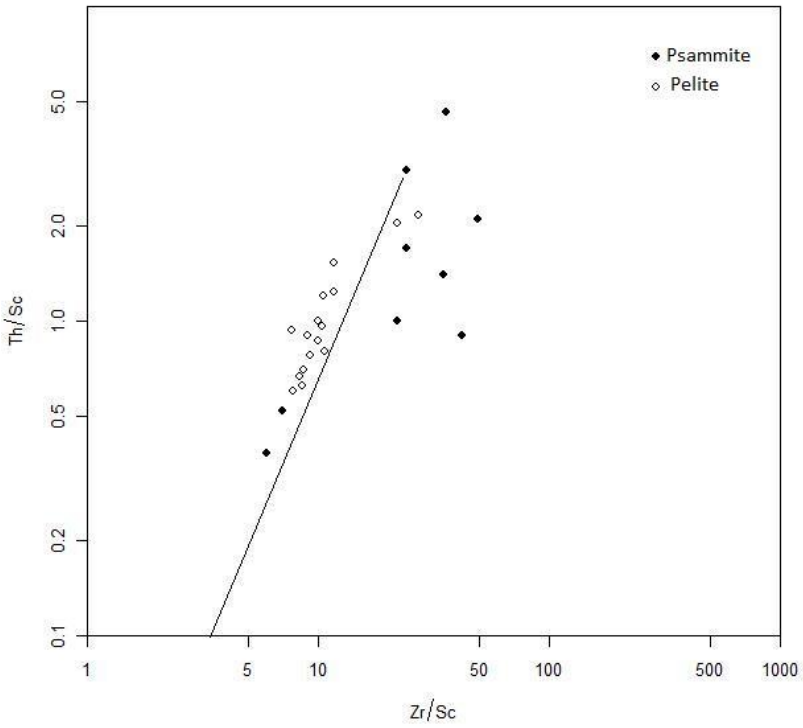
Psammite
Pelite
Th/Sc
5.0
2.0
1.0
0.5
0.2
0.1
1
5
10
50
100
500
1000
Zr/Sc

Figure. 4

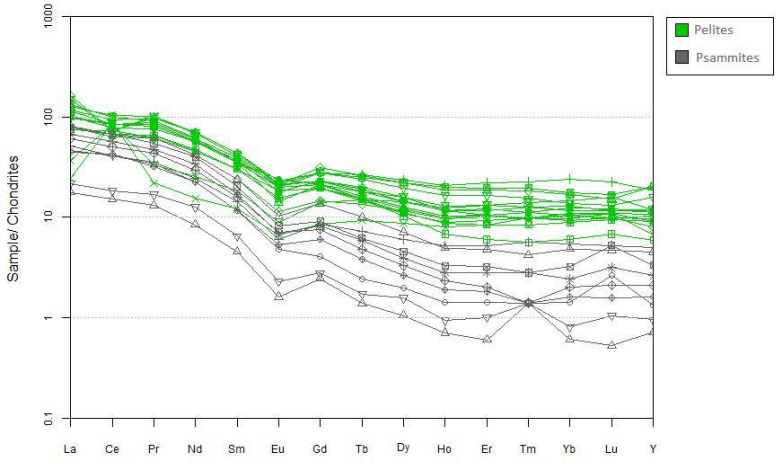

Figure. 5

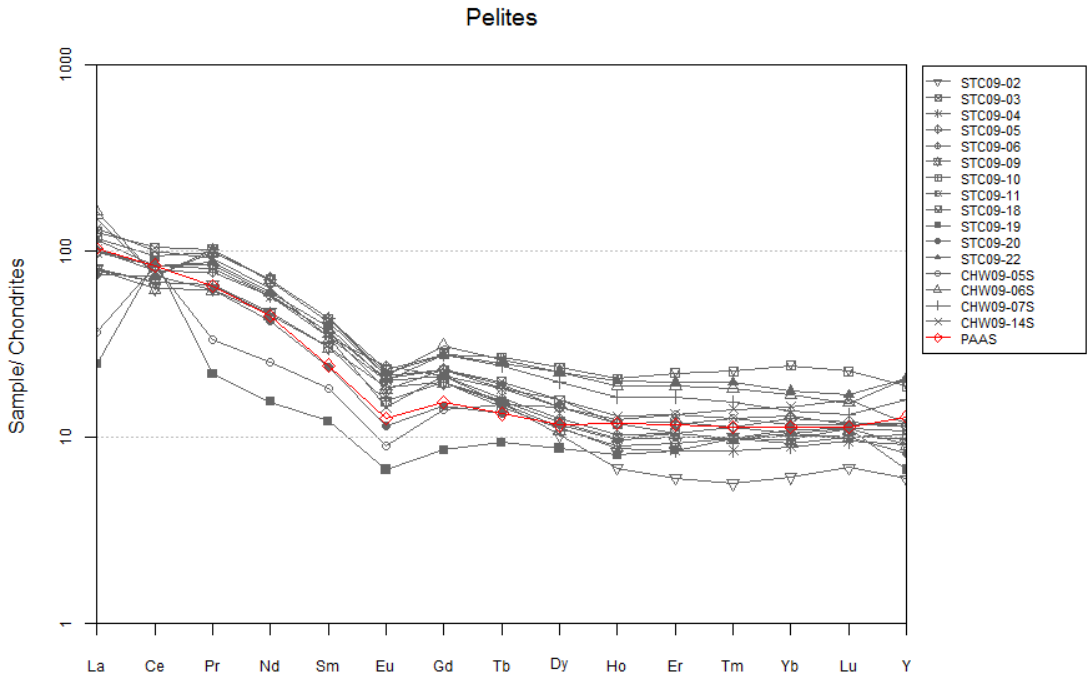

Figure. 6

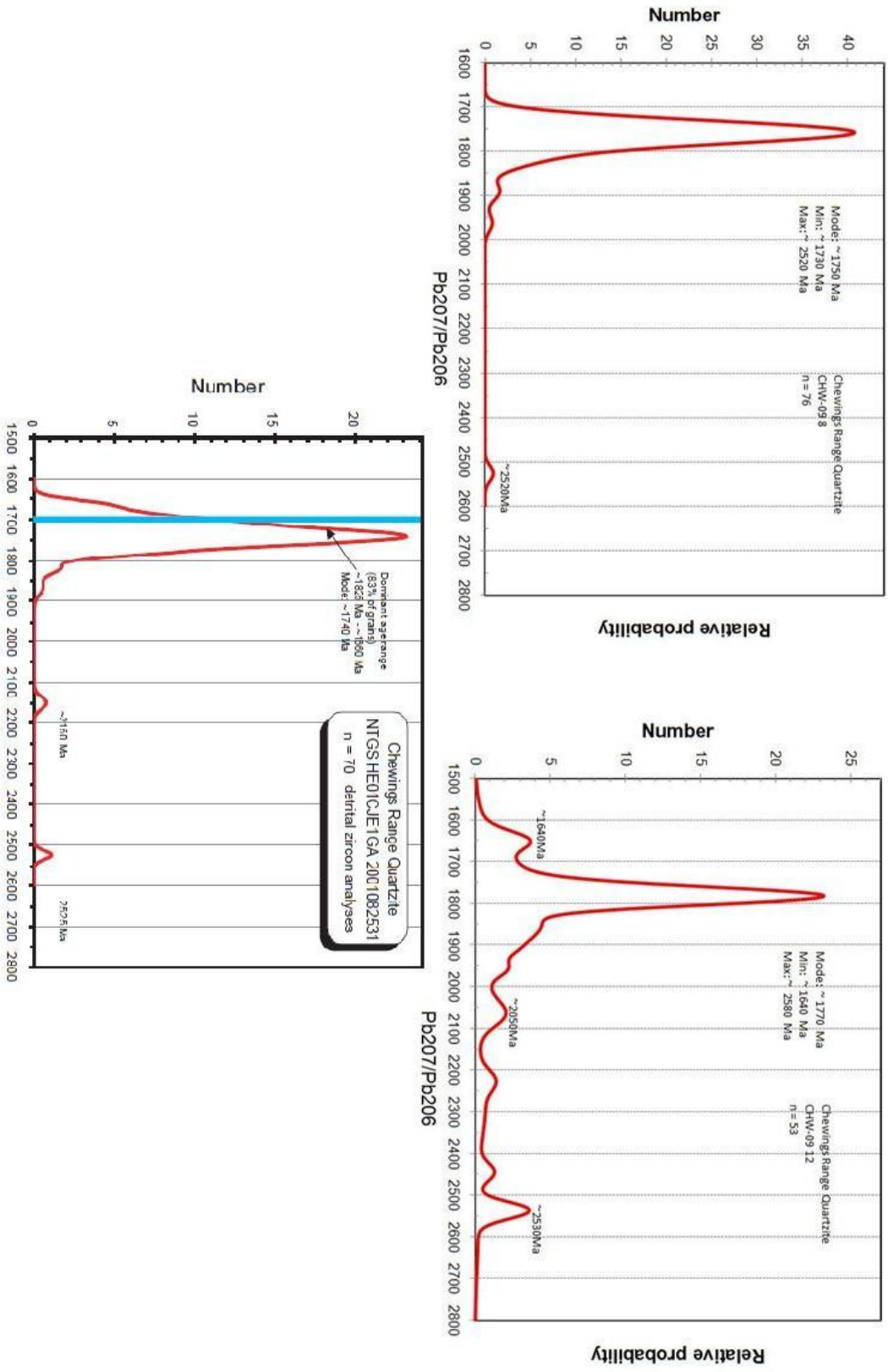
Number
Pb207/Pb206
Relative probability
Mode: ~1750 Ma
Min: ~1730 Ma
Max: ~2520 Ma
Chewings Range Quartzite
CHW-09 8
n = 76
~2520Ma
Number
Pb207/Pb206
Relative probability
Mode: ~1770 Ma
Min: ~1640 Ma
Max: ~2580 Ma
Chewings Range Quartzite
CHW-09 12
n= 53
~1640Ma
~2050Ma
~2530Ma
Number
Chewings Range Quartzite
NTGS:HE01CJE1GA 20010825J1
n = 70 detrital zircon analyses
Dominant age range
(63% of grains)
~1828 Ma - ~1860 Ma
Mode: ~1740 Ma

Figure. 7

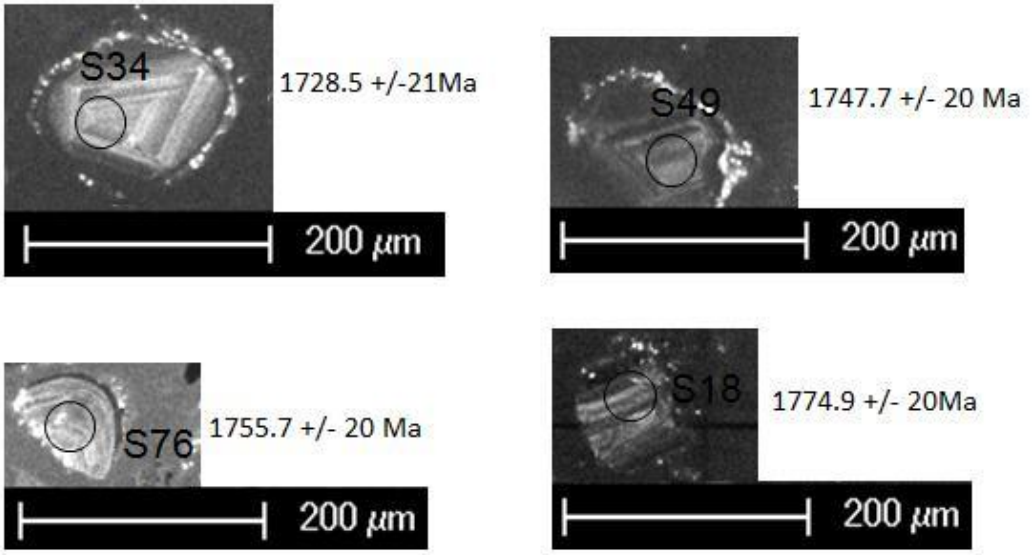
S34
1728.5 +/-21Ma
200 μm
S49
1747.7 +/- 20 Ma
200 μm
S76
1755.7 +/- 20 Ma
200 μm
S18
1774.9 +/- 20Ma
200 μm

Figure. 8

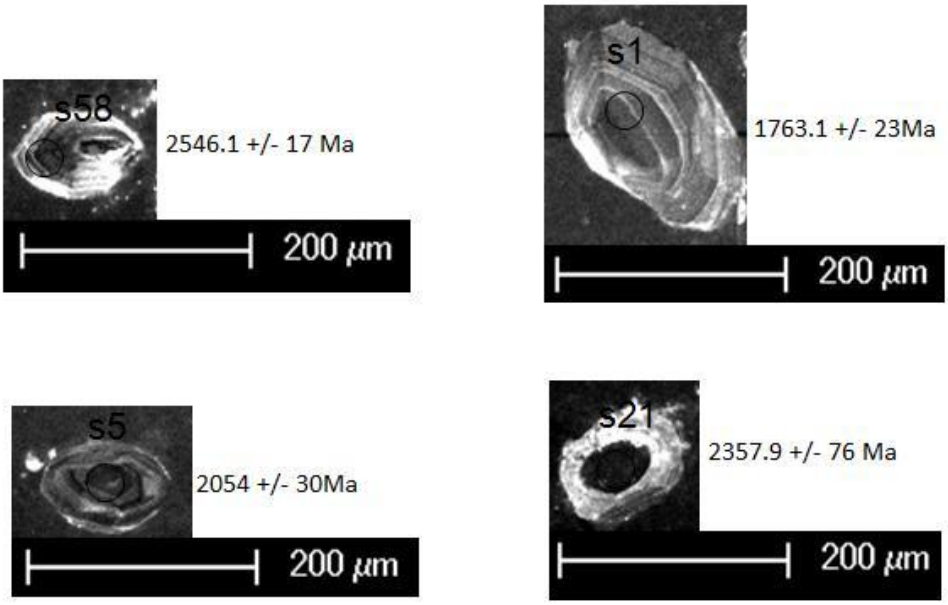
s58
2546.1 +/- 17 Ma
200 μm
s1
1763.1 +/- 23Ma
200 μm
s5
2054 +/- 30Ma
200 μm
s21
2357.9 +/- 76 Ma
200 μm

Figure. 9

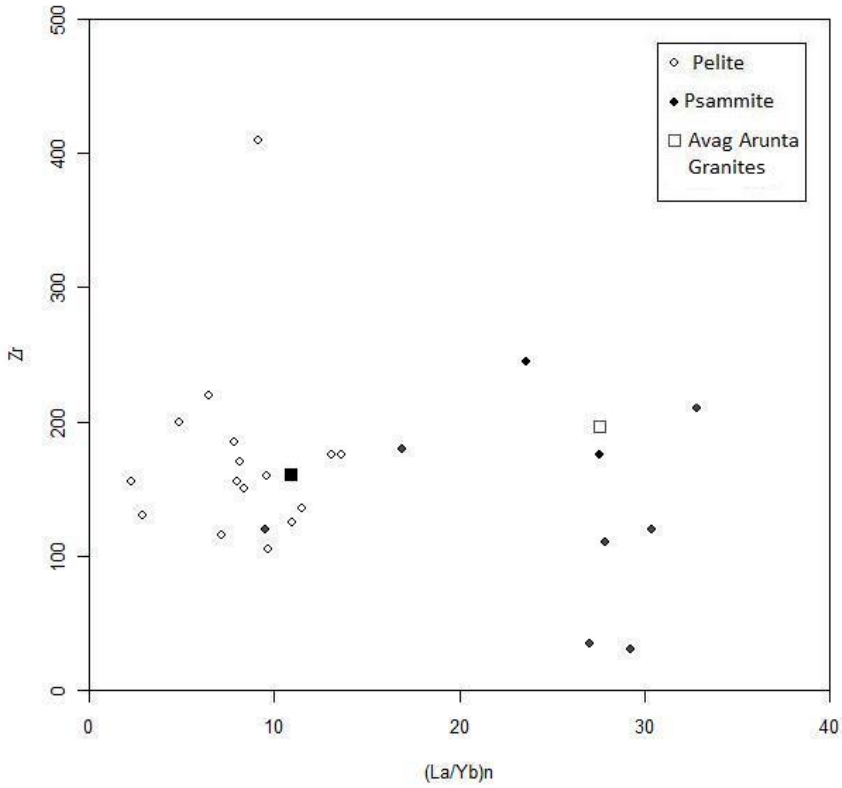

Figure. 10

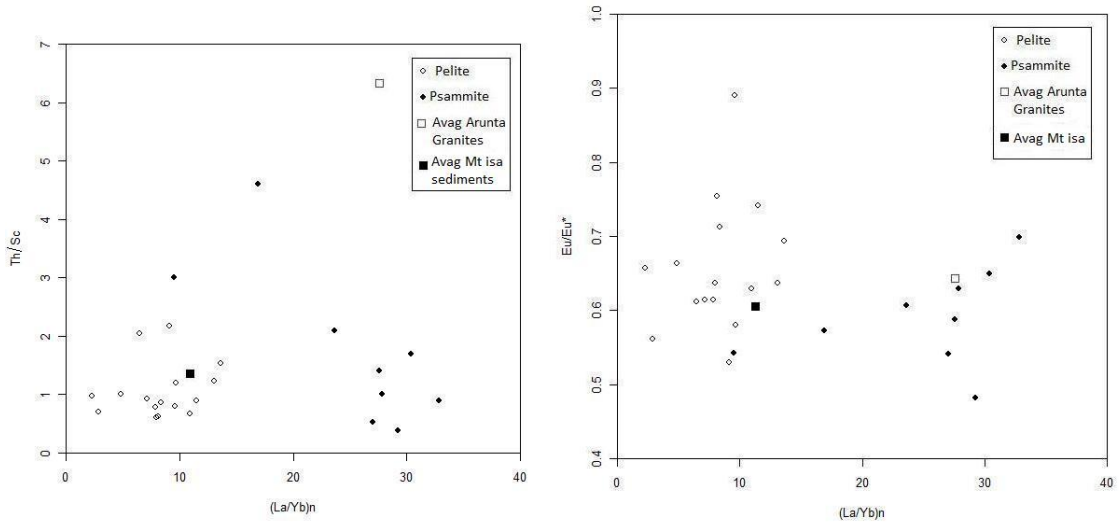

Figure. 11

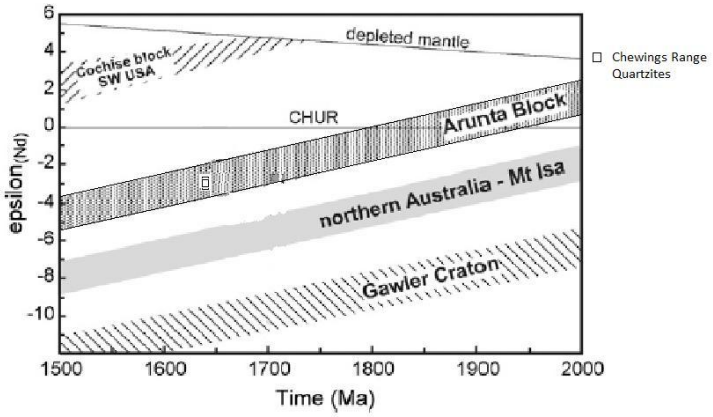
depleted mantle
Cochise block SW USA
CHUR
Arunta Block
northern Australia - Mt Isa
Gawler Craton
Chewings Range Quartzites
epsilon(Nd)
Time (Ma)
6
4
2
0
-2
-4
-6
-8
-10
1500
1600
1700
1800
1900
2000

Figure. 12

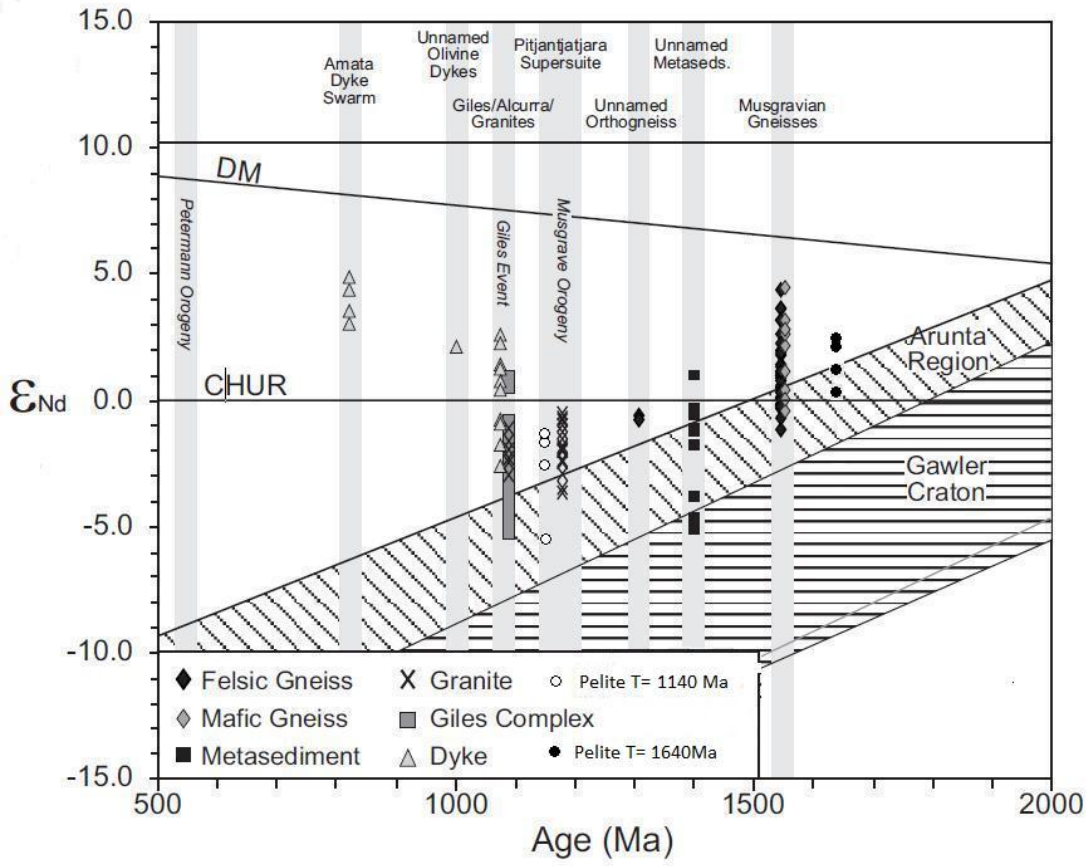
15.0
10.0
5.0
0.0
-5.0
-10.0
-15.0
εNd
500
1000
1500
2000
Age (Ma)
Amata Dyke Swarm
Unnamed Olivine Dykes
Pitjantjatjara Supersuite
Unnamed Metaseds.
Giles/Alcurra/ Granites
Unnamed Orthogneiss
Musgravian Gneisses
DM
CHUR
Petermann Orogeny
Giles Event
Musgrave Orogeny
Arunta Region
Gawler Craton
Felsic Gneiss
Mafic Gneiss
Metasediment
Granite
Giles Complex
Dyke
Pelite T= 1140 Ma
Pelite T= 1640Ma

Figure. 13

Table 1
Major and trace element analyses

	Chewings Range																	
	STC09-02	STC09-03	STC09-04	STC09-05	STC09-06	STC09-09	STC09-10	STC09-11	STC09-18	STC09-19	STC09-20	STC09-22	CHW09-05	CHW09-06	CHW09-07	CHW09-14	PAAS	
	(Pelite)	(Pelite)	(Pelite)	(Pelite)	(Pelite)	(Pelite)	(Pelite)	(Pelite)	(Pelite)	(Pelite)	(Pelite)	(Pelite)	(Pelite)	(Pelite)	(Pelite)	(Pelite)		
Major (wt%)																		
SiO2	65.2	69.8	66.8	62.5	67.8	62.9	65.6	63.7	59.1	57.3	61.1	68.8	67.6	70.3	66.5	59.3		
TiO2	0.765	0.76	0.685	0.875	0.72	0.83	0.77	0.77	1.01	0.71	0.635	0.67	0.67	0.51	0.63	0.79		
Al2O3	19.4	20.7	16.5	20.3	16.8	19.3	18	18.6	21.8	17.1	17.2	13	16.1	13.3	16.2	19.1		
Fe2O3	6.6	5.45	5.89	7.23	5.72	6.05	7.03	6.79	7.37	12.7	8.01	4.46	6.23	5.57	6.27	10		
MnO	0.03	0.06	0.09	0.15	0.09	0.08	0.15	0.15	0.12	0.06	0.06	0.1	0.06	0.06	0.09	0.05		
MgO	0.8	0.22	1.44	1.39	1.3	1.37	1.41	1.32	0.99	1.68	1.42	0.83	1.56	1.81	1.72	0.73		
CaO	0.12	0.07	0.74	0.63	1.2	1.12	0.86	0.8	0.21	0.53	0.53	0.21	0.23	1.27	0.27	0.08		
Na2O	0.16	0.04	1.16	0.86	2.09	2.02	1.05	1.19	0.67	0.42	0.58	1.52	0.91	1.64	0.92	0.14		
K2O	3.3	0.73	3.6	3.25	2.99	3.3	2.54	3.58	4.53	5.67	5.57	5.93	3.2	1.86	3.09	5.85		
P2O5	0.03	0.03	0.09	0.1	0.06	0.08	0.11	0.07	0.01	0.08	0.09	0.16	0.07	0.49	0.07	0.06		
LOI	3.75	2.65	2.29	2.69	2.27	2.46	2.53	2.14	4.54	3.95	5.68	0.84	3.64	3.02	3.69	3.09		
Total	100.155	100.51	99.285	99.975	101.04	99.51	100.05	99.11	100.35	100.2	100.875	96.52	100.27	99.83	99.45	99.19		
Trace and REE (ppm)																		
Ba	465	180	900	700	650	800	550	900	600	850	1100	750	650	390	650	700	650	
Co	45.5	46	125	80	65	60	85	70	40.5	55	65	60	55	120	85	24.5	23	
Cr	115	115	115	160	95	130	110	165	110	120	100	80	120	45	65	50	110	
Nb	14.5	13	11	12.5	11	12.5	11.5	11.5	16.5	13	12	12.5	9.5	10.5	8.5	7	19	
Ni	47	8	22	22	21	23	26	19	26	25	13	10	26	22	20	10	55	
Rb	170	38	190	165	140	140	145	170	245	265	280	305	175	110	180	345	160	
Sr	65	34.5	160	115	210	165	120	140	105	50	55	100	65	140	75	37.5	200	
Sc	15	15	15	20	15	20	20	15	20	15	15	10	15	10	15	15	16	
Th	18.5	23	13.5	15.5	12	12.5	12	13	20	14.5	14	20.5	10.5	12	10	32.5	14.6	
U	3.5	3	2	2.4	1.9	1.8	1.9	2.3	4.7	1.1	1.2	3.8	2.4	1.7	1.7	4.7	3.1	
Y	12.5	21.5	19	24	22.5	19	20.5	25	39.5	14	17	43	24	43	33.5	25	27	
Zn	80	75	34.5	75	33	41	70	75	33.5	110	95	75	105	105	95	34	85	
Zr	175	175	135	185	160	170	155	150	200	155	115	220	130	105	125	410	210	
Th/U	5.285714286	7.666667	6.75	6.458333	6.315789	6.944444	6.315789	5.652174	4.255319	13.18182	11.66667	5.394737	4.375	7.058823529	5.882352941	6.914893617		
La	29	46.5	37.5	36	37	29	29.5	36	43	9	27.5	42	13.5	60	55	48.5	38	
Ce	65	100	80	80	75	60	65	80	90	85	70	80	80	70	70	95	80	
Pr	9	14	11	11.5	10.5	8.5	9	11	13.5	3	8.5	12	4.6	13.5	14	12.5	8.9	
Nd	33.5	49	40.5	41.5	40.5	32.5	32.5	40.5	50	11	30	43	18	50	50	44.5	32	
Sm	7	9.5	8	8.5	8	7	7	8.5	10	2.8	5.5	9	4.2	10	10	8	5.6	
Eu	1.35	1.85	1.75	1.55	2.1	1.6	1.35	1.8	2	0.58	1	1.75	0.78	1.85	1.9	1.25	1.1	
Gd	6	7	6.5	7	6.5	6	6	7	8.5	2.6	4.5	8.5	4.3	9.5	8.5	6.5	4.7	
Tb	0.88	1.15	0.88	1.05	0.94	0.84	0.9	1.1	1.55	0.54	0.78	1.45	0.86	1.5	1.4	1.05	0.77	
Dy	3.9	6	4.3	5.5	4.8	4.2	4.6	5.5	9	3.3	4.4	8.5	5.5	8.5	7.5	6	4.4	
Ho	0.58	1	0.74	1	0.88	0.76	0.84	1	1.75	0.68	0.82	1.7	1.05	1.6	1.4	1.1	1	
Er	1.5	2.6	2.1	3	2.6	2.3	2.6	2.9	5.5	2.1	2.5	0.9	3.3	4.7	4.1	3.3	2.9	
Tm	0.2	0.35	0.3	0.4	0.4	0.35	0.35	0.45	0.8	0.35	0.35	0.7	0.45	0.65	0.55	0.5	0.4	
Yb	1.5	2.3	2.2	3.1	2.6	2.4	2.5	2.9	6	2.7	2.6	4.4	3.2	4.2	3.4	3.6	2.8	
Lu	0.26	0.38	0.36	4.6	0.42	0.42	0.38	0.44	0.86	0.42	0.38	0.64	0.44	0.58	0.5	0.6	0.4	
Eu/Eu*	0.636585253	0.693279	0.741624	0.614074	0.889949	0.754471	0.636585	0.713118	0.66293	0.656916	0.614271	0.611441	0.56089708	0.580039242	0.62978395	0.529731492		
(La/Yb)n	13.06448683	13.66189	11.51845	7.847411	9.616433	8.165304	7.973842	8.388612	4.84287	2.252498	7.147349	6.450334	2.85081744	9.653561697	10.93123898	9.103844989		
(Gd/Yb)n	3.241830065	2.46661	2.394534	1.830065	2.026144	2.026144	1.945098	1.956277	1.148148	0.780441	1.402715	1.565657	1.08905229	1.833177716	2.026143791	1.463326071		
Th/Sc	1.233333333	1.533333	0.9	0.775	0.8	0.625	0.6	0.866667	1	0.966667	0.933333	2.05	0.7	1.2	0.666666667	2.166666667		

Table 2
Major and trace element analyses

	Chewings Range										
	CHW09-01 (Psammite)	CHW09-02 (Psammite)	CHW09-04 (Psammite)	CHEW09-08 (Psammite)	CHEW09-10 (Psammite)	CHW09-11 (Psammite)	CHW09-12 (Psammite)	STC09-12 (Psammite)	STC09-21 (Psammite)		
Major (wt%)											
SiO2	92.7	82.5	84	87.9	90	90.7	93.8	97.8	99.1		
TiO2	0.09	0.28	0.205	0.2	0.13	0.15	0.06	0.025	0.045		
Al2O3	2.95	8.13	6.01	5.87	4.52	4.31	1.78	0.87	0.67		
Fe2O3	0.31	2.3	3.5	1.47	2.05	1.11	1.04	0.23	0.2		
MnO	<0.01	0.01	0.02	<0.01	<0.02	<0.03	0.03	<0.01	<0.02		
MgO	<0.01	0.16	0.16	0.03	<0.01	0.02	<0.01	<0.02	<0.03		
CaO	0.03	0.02	0.03	0.07	0.03	0.01	0.01	0.05	0.04		
Na2O	0.08	0.13	0.06	0.02	0.01	0.04	<0.01	0.02	0.02		
K2O	0.74	2.49	1.96	0.27	0.14	0.36	0.08	0.13	0.1		
P2O5	<0.01	0.01	<0.01	0.01	0.02	0.02	<0.01	<0.01	<0.02		
LOI	0.52	1.42	1.13	0.7	0.4	0.73	0.28	0.23	0.19		
Total	97.42	97.45	97.075	96.54	97.3	97.45	97.08	99.355	100.365		
Trace and REE (ppm)											
Ba	30	170	145	65	35	80	20	30	35		
Co	100	225	85	135	175	150	155	165	145		
Cr	45	45	40	85	95	70	125	125	115		
Nb	2	7	5.5	2.5	2	2.5	1	0.5	1		
Ni	<2	5	4	4	4	3	3	<2	<2		
Rb	39	145	90	17.5	8.5	25	5.5	7	6		
Sr	16.5	34	8.5	29	18.5	26.5	10.5	7	6		
Sc	<5	<5	<5	<5	<5	<5	<5	<5	<5		
Th	4.5	23	15	10.5	7	8.5	5	1.9	2.6		
U	0.8	3.2	1.3	1.6	1.3	0.9	0.6	0.6	0.4		
Y	2.8	9.5	10.5	7	5.5	4.4	3.4	1.5	2		
Zn	24	25	29	14	17	8.5	7	0.5	1.5		
Zr	210	180	120	245	175	120	110	30	35		
Th/U	5.625	7.1875	11.53846154	6.5625	5.384615385	9.444444444	8.333333333	3.16666667	6.5		
La	17	30	19	28	24.5	22.5	16.5	6.5	8		
Ce	39	65	39	65	55	48	40.5	14.5	17.5		
Pr	4.7	8.5	4.9	7.5	6.5	6	4.4	1.8	2.3		
Nd	16	30	17.5	28.5	24	21	16	6	9		
Sm	2.7	5.5	3.3	4.7	3.9	3.7	2.7	1.05	1.5		
Eu	0.42	0.9	0.52	0.72	0.6	0.62	0.42	0.14	0.2		
Gd	1.25	4.2	2.6	2.8	2.5	2.3	1.85	0.75	0.85		
Tb	0.14	0.58	0.42	0.36	0.34	0.28	0.22	0.08	0.1		
Dy	0.76	2.7	2.3	1.75	1.5	1.25	1	0.4	0.6		
Ho	0.12	0.42	0.44	0.28	0.24	0.2	0.16	0.06	0.08		
Er	0.35	1.2	1.3	0.8	0.7	0.5	0.45	0.15	0.25		
Tm	<0.05	0.15	0.2	0.1	0.1	0.05	0.05	<0.05	<0.05		
Yb	0.35	1.2	1.35	0.8	0.6	0.5	0.4	0.15	0.2		
Lu	0.1	0.18	0.2	0.2	0.12	0.08	0.06	0.02	0.04		
Eu/Eu*	0.698650304	0.572247587	0.542509253	0.606529603	0.587213989	0.649492828	0.62898101	0.48211451	0.54128047		
(La/Yb)n	32.82210977	16.89373297	9.510545968	23.65122616	27.59309718	30.40871935	27.8746594	29.2824705	27.0299728		
(Gd/Yb)n	2.89449113	2.836601307	1.560881143	2.836601307	3.376906318	3.728104575	3.74836601	4.05228758	3.44444444		
Th/Sc	0.9	4.6	3	2.1	1.4	1.7	1	0.38	0.52		

Sample	Sm (ppm)	Nd (ppm)	$^{147}Sm/^{144}Nd$	$^{143}Nd/^{144}Nd$	2S.E		εNd(0)[a]	εNd(T)[b]	Nd^{TDM}
Psammite									
CHW 09 - 1	2.2ppm	13.8ppm	0.10042	0.511401		7	-24.13	-3.91	2326 Ma
CHW 09 - 8	3.9ppm	22.8ppm	0.1052	0.511465		8	-22.88	-3.67	2339 Ma
CHW 09 - 9	3.9ppm	21.9ppm	0.10875	0.511494		8	-22.23	-3.86	2377 Ma
CHW 09 - 12	2.4ppm	13.9ppm	0.10388	0.511446		8	-23.25	-3.76	2337 Ma
STC 09 - 12	0.83ppm	4.9ppm	0.10242	0.511427		8	-23.62	-3.83	2333 Ma
Pelite									
CHW 09 - 14	9.1ppm	53ppm	0.10434	0.511659		8	-19.1	0.31	2056 Ma
STC 09 - 4	7.1ppm	37.1ppm	0.11563	0.511936		9	-13.69	3.35	1866Ma
STC 09 - 6	7.2ppm	38.4ppm	0.1144	0.511939		8	-13.64	3.66	1839 Ma
STC 09 - 18	9.8ppm	52.5ppm	0.1128	0.511863		8	-15.12	2.52	1923 Ma
For T= 1140Ma									
Sample	Sm (ppm)	Nd (ppm)	$^{147}Sm/^{144}Nd$	$^{143}Nd/^{144}Nd$	2S.E		εNd(0)[a]	εNd(T)[b]	Nd^{TDM}
Pelite									
CHW 09 - 14	9.1ppm	53ppm	0.10434	0.511659		8	-19.1	-5.65	2056 Ma
STC 09 - 4	7.1ppm	37.1ppm	0.11563	0.511936		9	-13.69	-1.88	1866Ma
STC 09 - 6	7.2ppm	38.4ppm	0.1144	0.511939		8	-13.64	-1.65	1839 Ma
STC 09 - 18	9.8ppm	52.5ppm	0.1128	0.511863		8	-15.12	-2.59	1923 Ma

Table. 3